clinic b_m parameter is associated with a switch of the polar moment in the perovskite sub-unit from the $[110]_p$ to the $[001]_p$ axis.

For each compound in the two-phase region near $x=0{\cdot}425$ the orthorhombic and tetragonal structures have a common Curie point, and presumably possess about the same free energy. An important feature of these phases, however, is that neither can transform directly into the other in a fashion analogous to the orthorhombic-tetragonal phase change occurring in $BaTiO_3$ at 0 °C. In the pseudo-cubic perovskite ferroelectrics the phase change proceeds fairly smoothly by a switch in the direction of the polar moment from the [110] axis to the nearest cube edge. A similar change is not likely to take place in the bronze structure, since if the strain effect in each small perovskite unit switched from the $[110]_p$ direction to one of the adjacent a_p-axes, this would give rise to an overall crystal symmetry lower than tetragonal. A change of strain direction from $[110]_p$ to the third, more remote cube axis, that is the c_p-axis in Fig. 5(*b*), is improbable because it would involve a relatively large energy change. In other words the strain directions $[110]_p$ and $[001]_p$ are frozen into different domains, so that orthorhombic and tetragonal structures coexist.

The properties of the $(Ba, Sr)Nb_2O_6$ solid solutions appear to be very similar to those of the $(Pb,Ba)Nb_2O_6$ compounds. The scale of the ferroelectric distortion effects is greatly reduced, however, compared with the (Pb, Ba) series, this being consistent with the lower Curie temperatures. This difference is very reminiscent of that between $BaTiO_3$ and $PbTiO_3$, and may very well be due to the same cause—the role of Pb.

References

ANLIKER, M., BRUGGER, H. R. & KÄNZIG, W. (1954). *Helvetica Physica Acta*, **27**, 99.

COATES, R. V. & KAY, H. F. (1958). *Phil. Mag.* **3**, 1449.

FRANCOMBE, M. H. (1956). *Acta Cryst.* **9**, 683.

FRANCOMBE, M. H. (1958). Ph.D. Thesis, Univ. of London.

FRANCOMBE, M. H. & LEWIS, B. (1957). *J. Electronics* **2**, 387.

FRANCOMBE, M. H. & LEWIS, B. (1958*a*). *Acta Cryst.* **11**, 696.

FRANCOMBE, M. H. & LEWIS, B. (1958*b*). Patent Application No. 1700/58.

GOODMAN, G. (1953). *J. Amer. Ceram. Soc.* **36**, 368.

GOODMAN, G. (1957). U.S. Patent No. 2,805,165.

LEWIS, B. & WHITE, E. A. D. (1956). *J. Electronics*, **1**, 646.

MAGNÉLI, A. (1949*a*). *Ark. Kemi Min. Geol.* **1**, No. 22.

MAGNÉLI, A. (1949*b*). *Ark. Kemi Min. Geol.* **1**, No. 32.

MEGAW, H. D. (1957). *Ferroelectricity in Crystals*, p. 16. London: Methuen.

ROTH, R. S. (1957). *Acta Cryst.* **10**, 437.

ROTH, R. S. (1959). Amer. Phys. Soc. Meeting, New York.

SHIRANE, G. & HOSHINO, S. (1954). *Acta Cryst.* **7**, 203.

Acta Cryst. (1960). **13**, 140

Defects in the Crystal and Magnetic Structures of Ferrous Oxide

BY W. L. ROTH*

General Electric Research Laboratory Schenectady, New York, U.S.A.

(*Received* 19 *March* 1959 *and in revised form* 21 *April* 1959)

The defect structure of non-stoichiometric FeO (Wüstite) has been investigated by measuring the neutron scattering of powders quenched from the high temperature equilibrium state. The nuclear scattering shows the defects to consist of both cation vacancies in octahedral sites and interstitial cations in tetrahedral sites. The defects give rise to diffuse scattering which suggests the atomic arrangement in the vicinity of the defect is similar to that in magnetite. The average magnetic moment of iron atoms in normal positions, obtained by measuring the scattering of neutrons by the periodic arrangement of spins in the antiferromagnetic state, indicate the magnetic structure in the vicinity of the defect is paramagnetic. The model is supported by magnetic studies which demonstrated the existence at low temperature of a magnetic remanence in exchange contact with the antiferromagnetic structure.

The magnetic structures of MnO, FeO, CoO and NiO have been studied by neutron diffraction with emphasis directed toward understanding their relation to the crystal anisotropies and deformations which occur on magnetic ordering (Shull *et al.* 1951; Roth, 1958). The neutron scattering from ferrous oxide exhibits anomalies which are related to a defect structure, and they have been investigated further to ascertain the nature of the defects and their effects on the magnetic arrangement.

When equilibrium compositions of ferrous oxide are quenched to room temperature, a cubic (Wüstite) phase is formed in which the Fe/O ratio varies over

* The neutron diffraction studies were carried out at the Brookhaven National Laboratory, Upton, L.I., New York.

wide limits. From a study of the chemical composition and room temperature lattice parameter, Jette & Foote (1933) concluded that ferrous oxide was an iron deficient NaCl structure. Benard (1949), however, found that oxides with a minimum iron content were stoichiometric, and that oxides of higher iron content contained interstitial iron in solid solution. Recent X-ray investigations (Willis & Rooksby, 1953; Foster & Welsh, 1956) support the conclusion that ferrous oxide is iron deficient, and measurements of the iron selfdiffusion coefficients (Himmel *et al.*, 1953) are consistent with the notion that there are cation vacancies in the crystal.

At 198 °K., there is an ordering of the magnetic moments associated with the iron atoms, and ferrous oxide becomes antiferromagnetic (Bizette & Tsai, 1943). Neutron diffraction studies have shown that the magnetic moments are arrayed in ferromagnetic sheets parallel to (111) planes; the moment directions are perpendicular to the ferromagnetic sheets, and point alternately up and down in adjacent sheets (Fig. 1). Associated with the magnetic ordering, there is a slight elongation along the [111] direction and the crystal becomes rhombohedral. The low temperature X-ray experiments of Willis & Rooksby (1953) show the rhombohedral deformation at 90 °K. decreases as the iron content decreases.

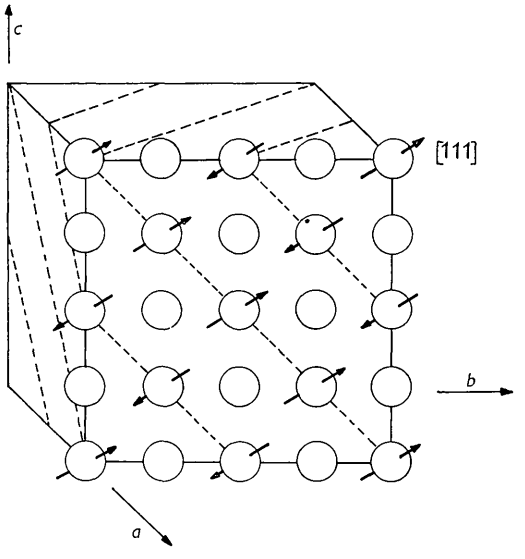

Fig. 1. Antiferromagnetic structure of FeO. The drawing describes the ideal crystal with atomic spins directed along the [111] axis.

Of particular interest are the consequences to the magnetic exchange interactions of introducing appreciable concentrations of vacancies into an antiferromagnetic structure. The magnetic structures of the series MnO, FeO, CoO and NiO can be interpreted as resulting from superexchange (Kramers, 1952; Anderson, 1950) in which there is negative exchange coupling between next-nearest magnetic neighbors. The substitution of a cation vacancy will perturb the superexchange coupling between the vacancy site and the six next-nearest neighbor cation sites. In addition, the presence of a cation vacancy in FeO implies the creation of two Fe^{+3} ions, and consequently there may be positive (ferromagnetic) double exchange (Zener, 1951) between Fe^{+2} and Fe^{+3} ions in the vicinity of the vacancy.

To elucidate the role of cation vacancies in ferrous oxide, neutron diffraction studies were made of specimens of varying composition in the paramagnetic state in order to confirm, if possible, the presence of cation vacancies and to investigate the possibility that the vacancies are ordered. Neutrons have an advantage over X-rays for this purpose because the nuclear scattering amplitudes of iron and oxygen are more nearly comparable. The specimens then were cooled and the magnetic scattering from the antiferromagnetic state measured. From these data were deduced the average occupancy and average magnetic moment associated with the cation sites, and comparison with the values calculated for the stoichiometric compound gives some insight into the effect of the vacancies on the magnetic exchange interactions.

Experimental

The ferrous oxide samples were prepared by Dr R. E. Carter and were the same as had been used in the previous work (Roth, 1958). The starting material was Johnson, Matthey Spectroscopic grade Fe_2O_3. Ten grams of powder, spread out in thin layers in platinum boats, were heated for 24–72 hr. in a controlled H_2O–H_2 atmosphere, then quenched by drawing into a water cooled tube which was flushed with dry N_2. X-ray diffraction patterns were made from each 10 g. sample and if the pattern showed the presence of Fe_3O_4 or Fe_2O_3 (indicating the quench was too slow) the equilibrium and quench was repeated. The aliquots were combined, powdered and sieved together to form homogeneous 100 g. specimens.

Specimen I was heated at 1000 °C. in $H_2O/H_2 = 0{\cdot}897$. From the equilibrium data (Darken & Gurry, 1946), a composition $FeO_{1.058} = Fe_{0.944}O$ was expected. All of the diffraction peaks could be indexed on a face-centered-cubic cell and the lattice parameters of the ten aliquots ranged from 4·302 to 4·306 Å. Interpolating from the data of Jette & Foote (1933), an $a_0 = 4.304$ Å corresponds to the composition $Fe_{0.934}O$, whereas from Benard's data one obtains $Fe_{0.975}O$. To discriminate between these estimates, a 1 g. sample was ignited to Fe_2O_3 and from the gain in weight the composition was $Fe_{0.940}O$, in essential agreement with Jette & Foote.

Specimen II was heated at 1000 °C. in the atmosphere $H_2O/H_2 = 1{\cdot}81$. From the equilibrium data the intended composition was $FeO_{1.086} = Fe_{0.926}O$. From the X-ray data, $a_0 = 4{\cdot}294$ Å which corresponds to $Fe_{0.918}O$ (Jette & Foote). In addition to the cubic

Wüstite lines, the X-ray patterns showed the presence of a crystalline phase we have been unable to identify. Estimating from the intensities of the X-ray peaks, there probably was about 5% of the unidentified phase relative to FeO.

The neutron diffraction measurements were made with the General Electric Spectrometer located at the Brookhaven National Laboratory Reactor. Since the diffuse scattering was of particular interest, the room temperature neutron diffraction patterns were accompanied by the measurement of the environmental background. The powder specimen, contained in a glass sample holder, was mounted in a cradle at the spectrometer center. At regular intervals, usually about every four counting cycles which corresponded to $\frac{1}{2}°-2\theta$, the entire sample holder automatically was displaced from the neutron beam and the background measured. The residual intensity, after subtracting background, is due exclusively to scattering from the specimen and the negligible scattering from the glass walls of the sample holder. For the low temperature measurements, the samples were in thin walled aluminum cylinders contained in a cryostat; patterns were obtained at 90 °K. and 4·2 °K., but independent background measurements could not be made.

Room temperature neutron scattering

At room temperature ferrous oxide is paramagnetic and the sharp Bragg peaks are the result of the neutron scattering from the periodic nuclear structure. In addition, non-Bragg scattering is observed which contains both nuclear and magnetic components. The patterns obtained from the two compositions are qualitatively similar and that for FeO–I is shown in Fig. 2. The variation of environmental background has been subtracted to give the true intensity curve. By this procedure most of the spurious detail was eliminated. For reasons which will be apparent later, it is desirable to index the neutron diffraction patterns on the basis of a unit cell whose dimensions are double those observed by X-rays, thus the usual (111), (200)... peaks are here indexed by (222), (400) ..., corresponding to a cubic cell with $a_0=8{\cdot}60$ Å.

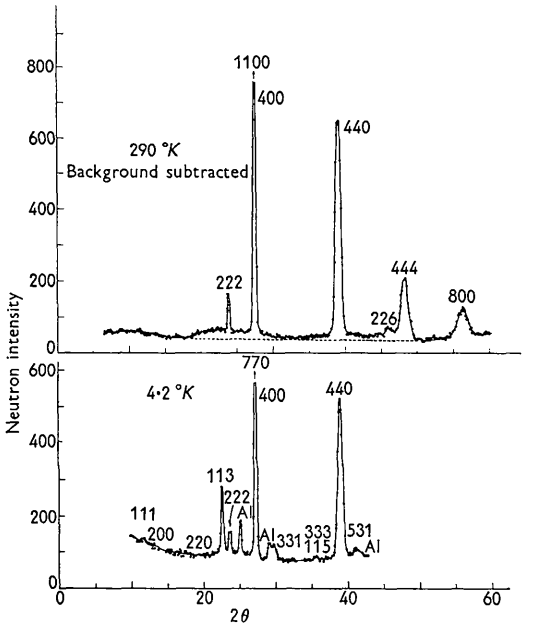

Fig. 2. Neutron diffraction patterns from FeO–I at 290 °K. and 4·2 °K. At 290 °K. the sample was in a flat glass holder and the background was measured by the sample in-out method. At 4·2 °K. a cylindrical aluminum holder was used and the impurity peaks are the 111 and 200 reflections from aluminum.

For a sodium chloride like structure, the (400) peak corresponds to iron and oxygen atoms scattering in phase, and (222) corresponds to scattering with a 180° phase difference. If $p=$the probability that on the average an iron atom site is occupied, then the ratio of neutron scattering in the (400) and (222) peaks is given by:

$$R=K(pf_{\mathrm{Fe}}+f_{\mathrm{O}})^2/(pf_{\mathrm{Fe}}-f_{\mathrm{O}})^2\,,$$

where $f_{\mathrm{Fe}}=0{\cdot}96\times10^{-12}$ cm., $f_{\mathrm{O}}=0{\cdot}58\times10^{-12}$ cm. are the nuclear scattering amplitudes, and K is a constant which includes the multiplicities, Lorentz, absorption and temperature factors. For $p=1$ the calculated ratio is 9·5 and R increases with decreasing values for p.

The nuclear intensities expected for stoichiometric FeO have been calculated and summarized in column A in Table 1. The observed values of R are 13·5 for I and 15·7 for II, clearly showing the absence of iron atoms at iron sites; these ratios correspond to the fractional occupancy of iron sites $p_{\mathrm{I}}=0{\cdot}92$ and $p_{\mathrm{II}}=0{\cdot}90$. Assuming the cation vacancies are distributed randomly in accordance with these averages, the integrated neutron intensities for the remaining Bragg peaks have been computed and the result is shown in column B. The data have been placed on an absolute scale by measuring with the identical experimental arrangement the neutron scattering from a standard specimen of nickel ($f_{\mathrm{Ni}}=1{\cdot}03\times10^{-12}$ cm.). The intensities are to be compared on an absolute basis and clearly agreement is improved by the introduction of cation vacancies.

There are several reasons for believing this simple vacancy model requires refinement: the concentration of iron atoms in the ferrous oxide specimens, as determined by chemical means, is 20% greater than calculated from the neutron scattering; in addition the cation vacancy model does not account for the observation that the (440) intensity is greater than that of (400). Finally, it is unlikely that 10% vacancies could be maintained in random solid solution since at that concentration 5% of the vacancies would have a vacancy as a nearest neighbor.

It is reasonable to expect that the excess iron atoms are located in the tetrahedral interstices of the rock salt structure. To treat this problem, we take the space

Table 1. *Nuclear scattering from ferrous oxide at* 290 °K.

	Integrated intensity							
	I (O/Fe = 1·058)				II (O/Fe = 1·086)			
hkl	*A*	*B*	*C*	Obs.	*A*	*B*	*C*	Obs.
111			1				3	
220			11				10	
113			41				45	
222	188	138	95	100	173	115	75	76
400	1695	1580	1342	1348	1550	1411	1192	1196
331			0				1	
422			6				6	
333, 115			20				22	
440	1548	1443	1445	1449	1372	1248	1250	1244
531			0				1	
620			4				3	
533			9				9	
226	131	97	66	58	114	76	49	59
444	630	588	500	549	542	493	417	463
511, 117			0				1	
642			5				4	
553, 731			18				18	
800	327	305	306	306	273	248	248	248

		I		II	
		P_b	P_d	P_b	P_d
A	Stoichiometric FeO	0	1	0	1
B	Cation vacancies only	0	0·92	0	0·90
C	Vacancies and interstitials	0·25	0·77	0·25	0·73

group O_h^7–$Fd3m$ which has the required cubic symmetry and provision for placing atoms in both the normal and interstitial positions. The unit cell contains a nominal 32 FeO and corresponds to the 'double cell' assumed previously. Placing the origin at the center of symmetry, the oxygen atoms are in 32(*e*) with $X=\frac{1}{4}$, corresponding to perfect cubic close packing. The cations are distributed among the two sets of positions 16(*c*) and 16(*d*) which correspond to the metal positions in the rock salt structure, and among 8(*a*) and 8(*b*) which are interstitial positions in which the cation is surrounded by a tetrahedron of oxygen atoms. For convenience, 8(*a*), (*b*) and 16(*c*), (*d*) will be termed tetrahedral and octahedral positions, respectively.

Let P_a, P_b, P_c, P_d be the probability that an *a*, *b*, *c*, or *d* site is occupied by an iron atom. For the rock salt structure (Model *A* in Table 1) $P_a=P_b=0$ and $P_c=P_d=1$, whereas for Model *B*, $P_a=P_b=0$ and $P_c=P_d=0{\cdot}92$ and 0·90 for specimens I and II, respectively. As vacancies and interstitials are distributed among the octahedral and tetrahedral sites, it should be noted that the occupancy of a particular octahedral site alters the probability that an *a* or *b* site is occupied. Thus if an octahedral position in 16(*c*) is filled, because of electrostatic repulsion between cations it is unlikely that the nearest tetrahedral sites in 8(*a*) will be occupied and the interstitial iron probably will go into an 8(*b*) position. Thus, as long as the deviation from stoichiometry is not too great, we assume:

$$P_c=1, \quad P_a=0$$

and consequently

$$16P_d+8P_b=n-16\,,$$

where n is the total number of iron atoms in the unit cell.

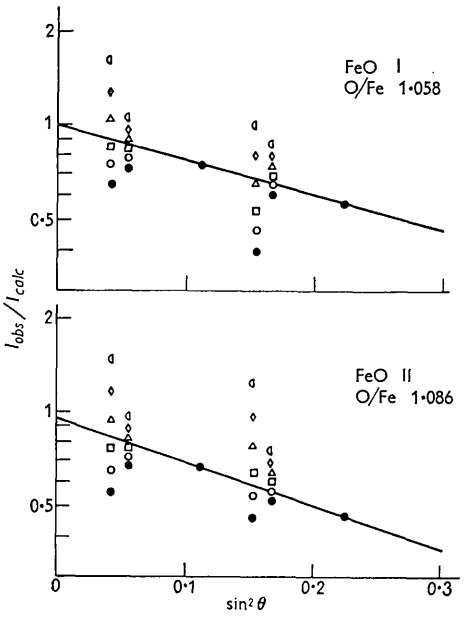

Fig. 3. Temperature-factor plots for coherent nuclear scattering from FeO. The data are on an absolute scale and I_c is shown for P_b: 0 = ●; 0·1 = ○, 0·2 = □, 0·3 = △, 0·4 = ◇, 0·5 = D.

Since n is known for each specimen, the neutron intensities can be evaluated for various values of P_b.

The results are shown in Fig. 3 where $\log (I_o/I_c)$ is plotted versus $\sin^2\theta$ and P_b is varied from 0 to 0·5. Since the intensities are on an absolute scale, a straight line which extrapolates to unity at $\sin^2\theta=0$ should be obtained. Satisfactory agreement for both specimens is obtained for $P_b=0{\cdot}25$, and the computed intensities are summarized in Table 1, column C. The extrapolation to $\sin^2\theta=0$ confirms the absolute intensity scale for I, whereas the extrapolated value for II shows the absolute scale is about 5·6% too large, in agreement with the presence of the second phase impurity which was noted in the X-ray examination. The values of the temperature factor B in the equation

$$I_o=I_c \exp(-2B \sin^2\theta/\lambda^2)$$

for the two specimens are:

$$2B_{(I)}=2{\cdot}66\times10^{-16} \quad \text{and} \quad 2B_{(II)}=3{\cdot}31\times10^{-16}.$$

Diffuse scattering

If the interstitial positions were occupied in a regular fashion, the space group $Fd3m$ requires scattering into Bragg peaks which are forbidden for the pure rock salt arrangement. The intensities calculated for these peaks are included under C in Table 1, and it can be seen that several, such as (113) and (220), are sufficiently strong to be detected. Sharp superlattice reflections are not observed either in the X-ray or neutron diffraction powder patterns, but those angles for which large intensity is calculated correspond to regions of intense diffuse scattering. This suggests that the major contribution to the diffuse scattering is the structural disorder created by the more or less random choice of different sets of tetrahedral sites available for occupancy by interstitial iron atoms.

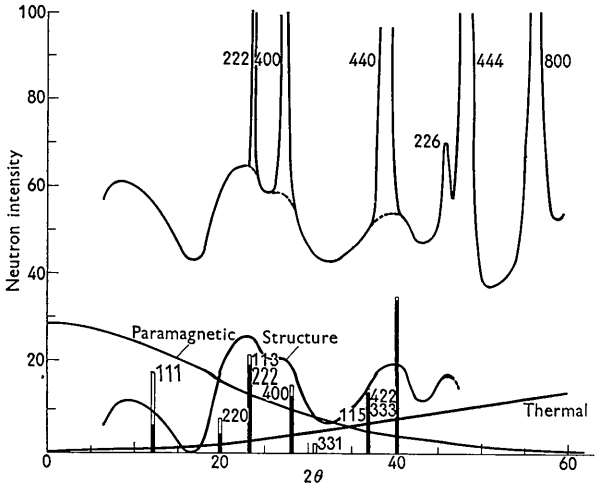

Fig. 4. Diffuse neutron scattering from FeO. The upper curve gives the total diffuse intensity after subtracting the environmental background. The lower curves show the resolved paramagnetic, thermal and structure imperfection diffuse scattering. (The isotropic multiple and isotope scattering are not shown.) The length of the solid and open bars is proportional to the nuclear and magnetic scattering from magnetite.

The expected sources for diffuse scattering of neutrons by ferrous oxide are the thermal motion of nuclei, paramagnetic scattering by the non-ordered atomic spins, imperfections in the atomic arrangement, and multiple scattering. Of particular interest is the structural diffuse component which is the result of scattering due to aperiodicities in the atomic arrangement brought about by positional disorder. This includes the effects of partial filling of tetrahedral interstices, clustering of interstices and vacancies, and local displacement of oxygen atoms as a consequence of the presence or absence of a cation in a particular octahedral or tetrahedral interstice. Since the multiple scattering is essentially isotropic, the angular dependent structural portion can be obtained by subtracting out the thermal and paramagnetic terms.

The results of such calculations are shown in Fig. 4. The environmental background has been subtracted out and the diffuse scattering plotted in the upper curve is due to the specimen only. The thermal and paramagnetic diffuse scattering were calculated from the equations:

$$F^2_{\text{thermal}}=\Sigma\{1-\exp[-2B(\sin\theta/\lambda)]^2\}b^2,$$
$$F^2_{\text{paramagnetic}}=2/3\,S(S+1)(e^2\gamma/(mc^2))f^2.$$

The temperature factor B was that obtained from the coherent Bragg scattering, and to compute the paramagnetic scattering a mean value of $S=1{\cdot}94$ was used, based on the fraction Fe^{+2} and Fe^{+3} present. The diffuse intensity scale was set by considering the structure diffuse scattering to be zero in the deepest minimum near 16° and the remainder of isotope and multiple scattering to be isotropic. The residual diffuse intensity represents the scattering due to structural disorder in the ferrous oxide crystal.* Since the diffuse intensity is due to crystal imperfections, it should be detected also by X-ray diffraction. This expectation has been confirmed by spectrometer traces using Cr $K\alpha$ radiation which show diffuse scattering in the same regions of reciprocal space as was observed with neutrons.

Low temperature neutron scattering

Below 200 °K. ferrous oxide is antiferromagnetic and the neutron diffraction pattern in Fig. 2 has additional peaks due to the scattering from the periodic magnetic structure. The magnetic structure of the 'ideal crystal' (Fig. 1) consists of ferromagnetic sheets parallel to (111) planes. The magnetic moments are normal to the ferromagnetic sheets and there is an alternation of spin direction in adjacent sheets. Of concern here are the consequences to the magnetic structure of the

* In some of the patterns there was a suggestion of further structure in the regions of diffuse scattering, but these peaks were within the precision of the counting statistics and could not be reproduced.

Table 2. *Neutron scattering from ferrous oxide at* 4·2 °K.

	Integrated intensity							
	I (O/Fe = 1·058)				II (O/Fe = 1·086)			
hkl	*A*	*B*	*C*	Obs.	*A*	*B*	*C*	Obs.
111	0	0	0	48	0	0	0	39
113	625	375	342	342	609	335	211	211
222	98	98	98	114	82	82	82	79
400	1375	1375	1375	1348	1295	1295	1295	1196
331	131	79	72	70	126	69	44	58
333, 115	46	28	35	31	44	24	15	ab.
440	1451	1451	1451	1451	1326	1326	1326	1330
$\langle \mu_B \rangle$	4	3·10	2·96		4	2·98	2·36	

$\langle \mu_B \rangle$ is average magnetic moment per octahedral site.
Intensity scales normalized with respect to {440} reflection from FeO–I.

presence of the cation defects. Below the magnetic ordering temperature, ferrous oxide deforms and becomes slightly rhombohedral, hence for a rigorous treatment, a rhombohedral space group should be used at low temperatures. However, the deformation could not be detected in the neutron experiments from powders, so to keep the discussion consistent with the distribution of atomic positions which was established in the high temperature cubic phase, the O_h^7–*Fd*3*m* description is retained.

The principal difference between the low and high temperature neutron diffraction patterns is additional Bragg scattering in the 113 and 331 reflections, and a small increase in scattering near 111. There is no significant change in either the diffuse scattering or the high temperature Bragg peaks, confirming the conclusion that these are due predominantly to nuclear scattering. Within experimental error, the neutron scattering at 90 °K. and 4·2 °K. is the same.

Except for the weak scattering near (111) the results are consistent with the antiferromagnetic structure previously described in which the spins are perpendicular to (111) planes. From the magnitude of the magnetic scattering, an estimate can be made of the average magnetic moment $\langle \mu_B \rangle$ per octahedral site. In Table 2 are given the calculated and observed intensities assuming several values for $\langle \mu_B \rangle$. Model *A* is the perfect stoichiometric crystal and the magnetic moment corresponds to the spin-only value of a ferrous ion, *B* is computed assuming the average moment is proportional to the fractional number of completed Fe–O–Fe bonds about each octahedral site, and *C* gives the intensities calculated based upon the average moment deduced from the intensity of the 113 reflection. From the magnetic intensities the average moment per octahedral site is $2{\cdot}96\mu_B$ for FeO–I (O/Fe = 1·058) and $2{\cdot}36\mu_B$ for FeO–II (O/Fe = 1·086), significantly smaller than the magnetic moments calculated for either *A* or *B*.

Discussion

The structure of ferrous oxide is conveniently regarded as a framework of oxygen atoms in cubic close packing with cations occupying the interstices. A single close packed layer is shown in Fig. 5, and in the stoichiometric compound, each of the 32 octahedral interstices designated by *c* would be occupied by an iron atom. In the non-stoichiometric compound, coulombic repulsion between cations in adjacent tetrahedral and octahedral sites will be minimized if the vacancies are directly associated with the interstitial cation.

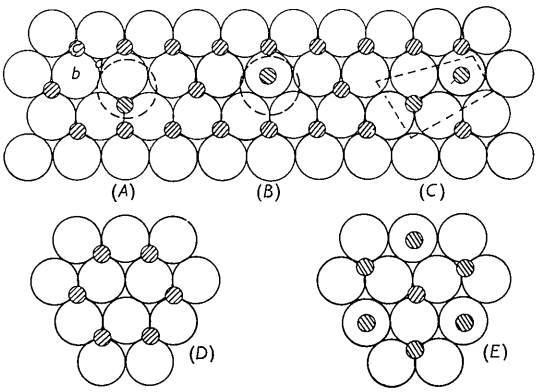

Fig. 5. Defect structure in FeO. A close packed plane is shown. ◍ and ◍ describe iron atoms in octahedral and tetrahedral positions. The (*a*) and (*b*) defects are equivalent, and (*c*) describes a cluster of two defects; (*d*) and (*e*) show layers in the atomic arrangement of Fe_3O_4.

The two sets of tetrahedral interstices are *a* and *b*, and two equivalent defects consisting of a tetrahedral cation and two octahedral vacancies are shown in Fig. 5(*A*) and (*B*). Because of repulsion between the interstitial cation and those in the nearest neighbor octahedral sites, the interstitial ion probably will be displaced to a position intermediately between the two tetrahedral sites. The vacancies are shown each carrying a positive charge to maintain electrical neutrality. The repulsion between cations in tetrahedral and octahedral sites can be further reduced by the coalescence of defects such that an octahedral vacancy is shared by two interstitial cations as shown in Fig. 5(*C*).

The coalescence of defects is a step toward the for-

Table 3. *Cation defects in ferrous oxide*

		I	II
Fe_xO	x	0·945	0·926
Content of average unit cell	n_{oxygen}	32	32
	n_{cation}	30·2	29·6
	n_c	16·0	16·0
	n_d	12·2	11·6
	n_b	2·0	2·0
	Fe^{+3}	3·5	4·7
Ratio of vacancies to interstitial cations		1·9	2·2
Fraction octahedral sites occupied		0·88	0·86
Next-nearest-neighbor shell	vacancies	0·71	0·83
	cations	5·29	5·17
	Fe–O–Fe bonds	4·66	4·46
	%Fe–O–Fe bonds	77·6	74·3
Average moment per octahedral site	calc.	$3{\cdot}10\mu_B$	$2{\cdot}98\mu_B$
	obs.	$2{\cdot}96\mu_B$	$2{\cdot}36\mu_B$

mation of Fe_3O_4, in which only 16 of the octahedral sites and 8 of the tetrahedral sites are occupied by cations. The structure of Fe_3O_4 is obtained by alternating layers of the type Fig. 5(*D*) and (*E*) in cubic close packing. Each occupied tetrahedral site is surrounded by four vacant octahedral positions disposed at the corners of a tetrahedron, so arranged that each vacancy is shared by two tetrahedral cations so that there is an average of 2 vacancies per interstitial. The close relation between Wüstite and magnetite is shown by the correspondence of the unit-cell dimensions which are 8·59 Å for $Fe_{30}O_{32}$ and 8·39 Å for $Fe_{24}O_{32}$.

The distribution of cations among the various crystallographic sites in non-stoichiometric FeO has been calculated from the neutron diffraction measurements and summarized in Table 3. There are two vacancies per interstitial cation, the same as is present in magnetite. This suggests the cation distribution in the vicinity of defects in Wüstite is similar to that in magnetite, and raises the question as to whether it is appropriate to regard them as small coherent volumes of magnetite in a Wüstite matrix. The defects are probably nuclei of the magnetite phase since when the rate of quenching to low temperature is slightly retarded, appreciable concentrations of magnetite are formed as a second phase. The structure dependent portion of the diffuse scattering in Fig. 4 is essentially the diffraction pattern of the defect. For comparison purposes, we have taken from the paper by Shull, Wollan & Kehler (1951) the calculated nuclear and magnetic neutron diffraction pattern for magnetite. There is rough agreement in the sense that large concentrations of diffuse scattering occur at angles corresponding to strong magnetite peaks. The patterns differ somewhat in detail, however; for example, the (111) peak is appreciably displaced in angle. If it is assumed that the diffuse pattern is that of magnetite, an estimate from the usual line broadening equation gives 8 Å for the average 'crystallite size.' Since this is less than the size of a single unit cell, the description is not significant, and it appears more appropriate to describe the defects in terms of clusters such as shown in Fig. 5(*A*), (*B*) and (*C*). This problem will be returned to when the magnetic interactions within the defect are considered.

The existence of interstitial cations in ferrous oxide is consistent with the observations of cation diffusion (Himmel *et al.*, 1953) in ferrous oxide. In the close packed oxygen structure, the diffusion path from a filled to vacant octahedral site is through a tetrahedral interstice. If the Wüstite specimen is regarded as a frozen-in distribution of the high temperature equilibrium, the defect concentration observed by neutrons is related to the concentration of interstitials at high temperature.

During the quenching process a specimen spends a finite time at a range of temperature where diffusion may occur and consequently represents a mixture of equilibrium distributions. This may account for the widely varying results obtained in studies on Wüstite noted by Foster & Welch (1956). In this regard, it should be noted that since there are both cation vacancies and interstitials in FeO, if the vacancy/interstitial ratio varies the simple specification of composition does not give a unique description of a specimen.

The discussion of the magnetic consequences of the cation defects is best introduced by considering the exchange interactions in a hypothetical perfect crystal. By analogy to MnO, NiO and CoO, we take the predominant magnetic interaction to be antiparallel superexchange between moments on next-nearest neighbor cations connected by oxygen anions:

$$\underset{\uparrow}{Fe^{+2}}\text{–O–}\underset{\downarrow}{Fe^{+2}}\text{–O–}\underset{\uparrow}{Fe^{+2}}\text{–O–}\underset{\downarrow}{Fe^{+2}}.$$

The moment per iron atom should be $2g\mu_B$ where the g-factor may be somewhat greater than 2.

The maintenance of electrical neutrality requires that the non-stoichiometry produced by a cation deficiency be accompanied by the formation of $2Fe^{+3}$ ions. Since the moment of Fe^{+3} is $5\mu_B$, if the Fe^{+3} ions occupy octahedral positions and antiparallel coupling between next-nearest-neighbors is retained, there will be only a slight decrease in the average

moment per octahedral site due to the smaller orbital contribution to the moment of Fe^{+3}. Alternatively, the double exchange (Zener, 1951) interaction Fe^{+2}–O–Fe^{+3} provides a mechanism for ferromagnetic coupling. The presence of cations in interstitial positions further allows of exchange between octahedral and tetrahedral sites since the $Fe_{(tet.)}$–O–$Fe_{(oct.)}$ angle is 135°. These sites are not crystallographically equivalent and hence a negative interaction is expected regardless of valence state. By analogy to the ionic distribution in magnetite, there may be a slight preference of Fe^{+3} for tetrahedral interstices, and the antiferromagnetic octahedral-tetrahedral exchange will result in a net ferrimagnetic moment.

This suggests that double exchange between differing valence states in octahedral positions and superexchange between ions in octahedral and tetrahedral positions may produce an uncompensated moment in the vicinity of the vacancy-interstitial defect complex. However, from the neutron diffraction experiments, only antiferromagnetic scattering is observed, and this is confirmed by the absence of an appreciable ferromagnetic remanence. The magnetization expected from the number of iron atoms associated with the vacancy-interstitial defects is much greater than the ferromagnetism which could possibly be present, consequently the spin correlation in the defect is antiferromagnetic or paramagnetic.

We next attempt to account for the observed average magnetic moment per octahedral site. The simple assumption that the moment is proportional to the concentration of iron atoms gives far too large a value. A somewhat better result is obtained by assuming the moment is proportional to the number of Fe–O–Fe bonds in superexchange contact. In a stoichiometric oxide, there are 6 next-nearest-neighbor cations in the first coordination sphere. For FeO–I 0·881 of the octahedral sites are occupied. Thus the number of Fe–O–Fe bonds is $0{\cdot}881\,(6\times 0{\cdot}881)=4{\cdot}66$ and 77·6% of the Fe atoms are in possible superexchange contact. Taking the g-value as 2, this corresponds to an average moment per octahedral site of $3{\cdot}10\mu_B$. A similar calculation for FeO–II gives $2{\cdot}98\mu_B$. These are minimal values since the calculated moments will be further increased by including an orbital contribution to the spin moment. The measured moments, based on the intensities of the 113 reflections, are $2{\cdot}96\mu_B$ and $2{\cdot}36\mu_B$.

The small magnetic moment observed by the neutron scattering shows that in FeO there is an appreciable concentration of atomic spins that are not ordered in the predominent antiferromagnetic structure. Further, they are not coupled so as to produce a ferromagnetic remanence. This suggests there are small 'paramagnetic' regions associated with the interstitial-vacancy defect complex. Taking $g=2$, we estimate the fraction of octahedral sites which contain cations whose spins are oriented in the antiferromagnetic structure to be 0·81 for I and 0·76 for II. Accordingly, about 20% of the octahedral sites are not contributing to the neutron scattering from the ordered structure, equivalent to a 'paramagnetic island' of approximately 2 interstitial cations plus 6 octahedral sites per unit cell.

The 'paramagnetic islands' have been defined by the fact that they do not produce coherent Bragg scattering associated with the 'ideal' magnetic structure. The regions may be 'super-paramagnetic' (Bean, 1955) in the sense that there is a ferromagnetic coupling but the volume is so small that thermal energy is sufficient to overcome the crystalline anisotropy and the magnetization of the 'island' will fluctuate in direction. A super-paramagnetic region will not possess a remanence, but might be observed by neutrons if the spin-reversal time were large with respect to the neutron passage time of about 10^{-13} sec. Estimates based on the magnetization behavior of single domain particles of iron (Néel, 1953) and the spin-lattice relaxation frequency in Fe_3O_4 (Galt *et al.*, 1953) indicate the spin-reversal frequency should be about 10^8–10^9 sec.$^{-1}$, hence a super-paramagnetic region should scatter neutrons coherently. The 'forbidden' intensity near (111) probably is of magnetic origin since it appears below the antiferromagnetic Néel temperature. If the anomalous intensity is due to super-paramagnetic scattering from N iron atoms with spins arrayed ferromagnetically in islands with random orientations of the magnetic axes, the calculation gives $N=1{\cdot}9$ atoms per 32 FeO cell. This is approximately the same as the number of occupied tetrahedral interstices, or about 6% of the cations in the crystal.

Magnetic exchange anisotropy

The magnetic structure in a $(11\bar{1})$ plane of Wüstite is described in Fig. 6. Three defect regions are shown, ranging from that about a single interstitial to a 'magnetite-like' block derived from the coalescence of six interstitial cations. Some idea of the distribution of defects in the matrix may be obtained from Fig. 7 which gives the distribution obtained by inserting interstitials in accordance with coordinates drawn from a table of random digits. Although most of the interstitials are isolated, there is an appreciable concentration of clusters containing two, three or more interstitial cations. The actual distribution will be peaked toward larger aggregates since energy considerations favor the growth of larger clusters. This may be seen by reference to Fig. 6, which shows that in the larger clusters the cations and vacancies can be arranged to reduce coulombis repulsion, whereas a single interstitial either is forced to occupy a high energy position between tetrahedral interstices, or to be surrounded by four vacancies. In the stoichiometric portion of the crystal, or 'matrix', every other spin along a closepacked direction is parallel and in the same magnetic sublattice. The M–O–M' angle between cations situated on octahedral and tetrahedral

sites is 135°, permitting superexchange coupling between interstitial and normal cations to produce a ferrimagnetic moment in the vicinity of the defect. Since the magnetization within the defect is coupled to that of the antiferromagnetic matrix, the proposed defect structure suggests the possibility of magnetic exchange anisotropy in the ferromagnetic component, similar to that observed in Co–CoO magnets by Meiklejohn & Bean (1957).

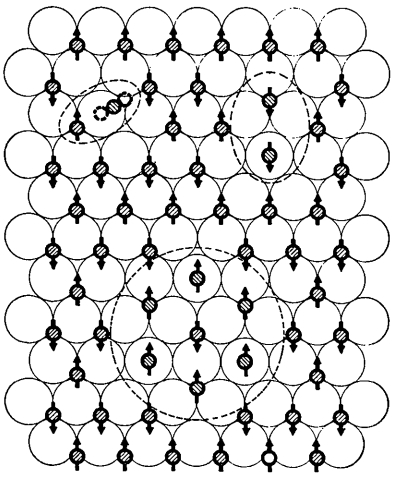

Fig. 6. Magnetic structure of defects. The projection on $(11\bar{1})$ of three clusters formed from 1, 2 and 6 interstitial cations is shown. The isolated interstitial occupies an intermediate position between tetrahedral interstices.

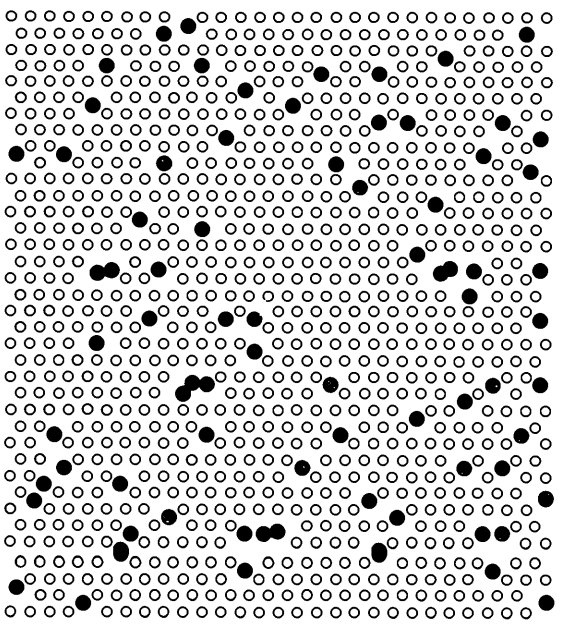

Fig. 7. The statistical distribution of clusters in (111) of FeO. The calculation is for the random insertion of interstitials, based on the composition O/Fe = 1·08 with two vacancies per interstitial cation.

The coexistence of ferromagnetic and antiferromagnetic regions, coherent in both an atomic and magnetic sense, has significant magnetic consequences. Magnetic studies (Roth, 1959) showed a small ferromagnetic remanence at room temperature.* The remanence increased with decreasing temperature, attained a maximum value then decreased as the temperature was further lowered from 4·2 to 2·1 °K. In addition, the hysteresis loop of a specimen which had been cooled to 4·2 °K. in a field of 12000 Ørsteds was found to be asymmetric and displaced by −2000 Ørsteds along the field axis.

These results support and extend the defect model deduced from the neutron scattering studies. Within the FeO crystal there is a distribution of clusters of defects, ranging in size from that of a single interstitial cation to larger aggregates with atomic arrangements approximating that of magnetite. The spins within each cluster are ferrimagnetically coupled, but at room temperature the applied magnetic field is able to orient the magnetization of only the larger clusters against the randomizing effects of thermal motion, i.e., the smaller clusters are superparamagnetic. As the temperature is lowered, increasingly smaller clusters can be lined up and the remanence increases. At still lower temperature (2·1 °K. for FeO–I) the exchange interaction between the antiferromagnetic matrix and the ferrimagnetic clusters overcomes that of the field. Since the applied field is no longer able to orient the ferrimagnetic moment, the remanence now will decrease (Kouvel *et al.*, 1958). In similar fashion, the shifted hysteresis loop (Meiklejohn & Bean, 1957) is the result of the unidirectional anisotropy developed when the antiferromagnetic and ferrimagnetic volumes are magnetically ordered by the applied field.

The author is indebted to R. E. Carter for specimen preparation, I. S. Jacobs and W. H. Meiklejohn for magnetic measurements, and A. Abrahamsen for technical assistance in the neutron diffraction experiments. Helpful discussions with J. S. Kouvel, W. H. Meiklejohn and Prof. F. C. Frank of the University of Bristol are gratefully acknowledged.

References

Anderson, P. W. (1950). *Phys. Rev.* **79**, 350.
Bean, C. P. (1955). *J. Appl. Phys.* **26**, 1381.
Benard, J. (1949). *Bull. soc. chim. Fr.* 109.
Bizette, H. & Tsai, B. (1943). *C. R. Acad. Sci., Paris*, **217**, 390.
Darken, L. S. & Curry, R. W. (1946). *J. Amer. Chem. Soc.* **68**, 798.
Foster, P. K. & Welsh, A. J. E. (1956). *Trans. Faraday Soc.* **52**, 1626.
Galt, S. K., Andrus, J. & Hopper, H. G. (1953). *Rev. Mod. Phys.* **25**, 93.

* The remanence in our sample of FeO powder was observed to increase after a year of storage at room temperature. This is believed to be due to the growth of larger clusters from single interstitials, but also may have resulted from slow atmospheric oxidation.

HIMMEL, L., MEHL, R. F. & BIRCHENALL, C. E. (1953). *Trans. Amer. Inst. Min. (Metall.) Engrs.* 827.
JETTE, E. R. & FOOTE, F. (1933). *J. Chem. Phys.* **1**, 29.
KITTEL, C. (1936). *Introduction to Solid State Physics*, 2nd Ed., p. 486. New York: Wiley.
KOUVEL, J. S., GRAHAM, C. D., Jr. & BECKER, J. J. (1958). *J. Appl. Phys.* **29**, 518.
KRAMERS, H. (1934). *Physica*, **1**, 182.
KRAMERS, H. (1952). *Physica*, **18**, 101.
MEIKLEJOHN, W. H. & BEAN, C. P. (1957). *Phys. Rev.* **105**, 904.
NÉEL, L. (1953). *Revs. Mod. Phys.* **25**, 293.
ROTH, W. L. (1958*a*). *Phys. Rev.* **110**, 1333.
ROTH, W. L. (1958*b*). *Phys. Rev.* **111**, 772.
ROTH, W. L. (1959). *J. Appl. Phys.* **30**, 303 S.
SHULL, C. G., STRAUSER, W. A. & WOLLAN, E. O. (1951). *Phys. Rev.* **83**, 333.
SHULL, C. G., WOLLAN, E. O. & KOEHLER, W. C. (1951). *Phys. Rev.* **84**, 912.
WILLIS, B. T. M. & ROOKSBY, H. P. (1953). *Acta Cryst.* **6**, 827.
ZENER, C. (1951). *Phys. Rev.* **82**, 403.

Acta Cryst. (1960). **13**, 149

The Crystal Structure of the Ethylene Complex *trans*-$[Pt(C_2H_4)(NH(CH_3)_2)Cl_2]$

BY P. R. H. ALDERMAN, P. G. OWSTON AND J. M. ROWE

Imperial Chemical Industries Limited, Akers Research Laboratories, The Frythe, Welwyn, Herts., England

(*Received* 1 *May* 1959 *and in revised form* 20 *May* 1959)

$[Pt(C_2H_4)(NH(CH_3)_2)Cl_2]$ is monoclinic, with the unit-cell parameters

$$a = 7{\cdot}77 \pm 0{\cdot}02,\quad b = 8{\cdot}67 \pm 0{\cdot}03,\quad c = 6{\cdot}65 \pm 0{\cdot}02\ \text{Å};\quad \beta = 102°.$$

There are two molecules in the unit cell (density observed 2·60, calculated 2·59 g.cm.$^{-3}$), and the space group is $P2_1/m$ or $P2_1$.

The [010] and [001] projections were studied, and the positions of the light atoms found by the systematic use of difference syntheses. The structure so derived has the symmetry $P2_1/m$, the principal plane of the molecule being a plane of symmetry.

It is confirmed that the ethylene molecule is symmetrically bound to the platinum atom. The carbon–carbon bond (1·47 Å) is longer than a normal double bond, though the significance to be attached to this lengthening depends on the method used to assess the errors. The bond-lengths Pt–Cl (2·30 and 2·33 Å) and Pt–N (2·02 Å) have normal values within experimental error, in spite of the high *trans*-effect of the ethylene ligand, and there is no '*trans*-lengthening' or '*cis*-shortening' of the bonds. The π-bonding theory of the *trans*-effect accounts for this result and also for the apparently contradictory observation of Bokii & Kukina (1957) that in the ion $[Pt(C_2H_4)Br_3]^-$ the bond lengths differ from their normal values.

The standard deviations of the bond-lengths were calculated from the diagonal elements only of the least-squares matrix to be CH_2–CH_2 0·18, Pt–Cl 0·04, Pt–N 0·19 Å, but this approximate method of estimating the errors may not be appropriate to this type of compound.

1. Introduction

The available evidence on the structure of ethylene complexes of platinum leads to the conclusion that they are π-complexes. The ethylene molecule is then bound to the metal by the donation of π-electrons from the ethylene ligand to the metal; there is also some back-donation of *d*-electrons from the metal to the anti-bonding orbitals of the ethylene (Chatt & Duncanson, 1953). This type of bonding can occur in the ion of Zeise's salt $[Pt(C_2H_4)Cl_3]^-$, the best-known π-complex, if the three chlorine atoms and the centre of the C–C bond occupy the four corners of a 'square-planar' arrangement round the platinum atom, and the two carbon atoms are arranged symmetrically above and below this plane.

Attempts to confirm this type of structure by X-ray methods have been made (Wunderlich & Mellor, 1954, 1955; Bokii & Kukina, 1957) and the positions of the heavier atoms found, but the coordinates of the carbon atoms were not found accurately. Two related compounds of palladium have also been studied (Dempsey & Baenziger, 1955; Holden & Baenziger, 1955), with results which also appeared to be in agreement with the proposed type of structure, though in $(Pd(C_2H_4)Cl_2)_2$ the carbon atoms appeared only rather indefinitely, and in (Pd styrene $Cl_2)_2$ the carbon–carbon bond is not perpendicular to the plane of the complex, presumably because the styrene molecule is not symmetrical about its double bond.

We therefore examined first the slightly simpler compound *trans*-$[Pt(C_2H_4)(NH_3)Cl_2]$, which proved to